Original papers
Nanostructured, nanoscale materials and nanodevices

УДК 544.174 DOI: 10.17277/jamt-2025-10-01-019-031

Influence of graphene oxide additives on the filler structure and the physical and mechanical properties of carbon-graphite nanocomposite

© Roman D. Balabanov[a,b]✉, Tatyana P. Dyachkova[a], Anna G. Fedyushkina[b], Irina V. Gutnik[a], Georgy A. Titov[a], Elena A. Burakova[a], Evgeny N. Tugolukov[a]

[a] *Tambov State Technical University, Bld. 2, 106/5, Sovetskaya St., Tambov, 392000, Russian Federation,*
[b] *JSC NIIgrafit, 2, Elektrodnaya St., Moscow, 111524, Russian Federation*

✉ balabanoff98@gmail.ru

Abstract: In this work, the influence of graphene oxide (GO) additives on the structure and morphology of graphite filler, as well as the strength characteristics of final carbon-graphite composites, is investigated. The formulation of prototype charge samples was selected using the mathematical method of experiment planning and the Hartley plan. The granulometric composition of the initial and modified charge samples, along with their adsorption capacity with respect to pitch, was determined. Scanning electron microscopy, Raman spectroscopy, XRD analysis, vibration density measurements, and specific surface area analysis (via BET) were used to evaluate the structure and morphology of the filler particles. It was found that when 0.9 wt. % GO is added to the filler composition, a denser grain structure with fewer voids is formed. At the same time, the specific surface area decreases by a factor of 3.6, while the sorption capacity for pitch, on the contrary, increases by a factor of 2.7, indicating a change in the chemical composition of the filler particle surfaces. According to Raman spectroscopy data, the modified charge samples exhibit a higher D/G ratio, the presence of functional groups on the particle surface, and a predominance of edge defects. Physical and mechanical testing of the samples after firing revealed that the introduction of 0.9 wt. % graphene oxide increases the compressive strength from 35.5 to 97.5 MPa. These results are significant for the development of new composite materials for tribotechnical applications.

Keywords: graphite; graphene oxide; antifriction materials; strength; mathematical modeling.

For citation: Balabanov RD, Dyachkova TP, Fedyushkina AG, Gutnik IV, Titov GA, Burakova EA, Tugolukov EN. Influence of graphene oxide additives on the filler structure and the physical and mechanical properties of carbon-graphite nanocomposite. *Journal of Advanced Materials and Technologies*. 2025;10(1):019-031. DOI: 10.17277/jamt-2025-10-01-019-031

Влияние добавок оксида графена на структуру наполнителя и физико-механические свойства углеграфитового нанокомпозита

© Р. Д. Балабанов[a,b]✉, Т. П. Дьячкова[a], А. Г. Федюшкина[b], И. В. Гутник[a], Г. А. Титов[a], Е. А. Буракова[a], Е. Н. Туголуков[a]

[a] *Тамбовский государственный технический университет, ул. Советская, 106/5, пом. 2, Тамбов, 392000, Российская Федерация,*
[b] *АО «НИИграфит», ул. Электродная, 2, Москва, 111524, Российская Федерация*

✉ balabanoff98@gmail.ru

Аннотация: Рассмотрено влияние добавок оксида графена (ОГ) на структуру и морфологию графитового наполнителя и прочностные характеристики конечных углеграфитовых композитов. Рецептурный состав опытных образцов шихты выбран с применением математического метода планирования эксперимента и плана Хартли. Определены гранулометрический состав образцов исходной и модифицированной шихты и их адсорбционная емкость по отношению к пеку. Для оценки структуры и морфологии частиц наполнителя использованы методы сканирующей электронной микроскопии, КР-спектроскопии, рентгеновской дифрактометрии, измерения

виброплотности и удельной поверхности (по БЭТ). Показано, что при добавлении 0,9 мас. % ОГ в состав наполнителя формируется более плотное зерно с меньшим количеством пустот. При этом значение удельной поверхности снижается в 3,6 раза, а сорбционная емкость по отношению к пеку, напротив, возрастает в 2,7 раза, что указывает на изменение химического состава поверхности частиц наполнителя. По данным спектроскопии КР образцы модифицированной шихты характеризуются более высоким значением соотношения D/G, на поверхности частиц присутствуют функциональные группы, преобладают краевые дефекты. В ходе физико-механических испытаний образцов после обжига установлено, что за счет введения 0,9 мас. % оксида графена предел прочности при сжатии увеличивается с 35,5 до 97,5 МПа. Полученные результаты имеют важное значение для разработки новых композитных материалов триботехнического назначения.

Ключевые слова: графит; оксид графена; антифрикционные материалы; прочность; математическое моделирование.

Для цитирования: Balabanov RD, Dyachkova TP, Fedyushkina AG, Gutnik IV, Titov GA, Burakova EA, Tugolukov EN. Influence of graphene oxide additives on the filler structure and the physical and mechanical properties of carbon-graphite nanocomposite. *Journal of Advanced Materials and Technologies*. 2025;10(1):019-031. DOI: 10.17277/jamt-2025-10-01-019-031

1. Introduction

The requirements for the physical and mechanical properties of tribotechnical materials used in modern equipment, transport systems, and technical devices operating under extreme conditions are extremely high [1, 2]. Particularly in demand are antifriction self-lubricating materials that include graphite, which possesses unique characteristics such as thermal and chemical stability, high conductivity, and excellent strength properties.

In the production of carbon-graphite materials, the main raw components used are coke, coal tar pitch, and natural graphite. The technological process consists of several key stages: cold pressing of a mixture of fine-dispersed carbon powders, thermal treatment at 1250 °C, followed by impregnation and graphitization, which occurs at temperatures ranging from 2300 to 2500 °C [3].

One of the drawbacks of graphite materials that limits their use in friction units is their susceptibility to oxidation in aggressive environments at temperatures above 400 °C [4, 5]. Various methods are used to address this issue, such as impregnation with phosphorus-containing compounds [6]. To reduce porosity and increase strength, graphite materials are impregnated with resins and metals [7–9]. Changes in the porosity and surface structure of graphite under conditions of liquid friction affect its tribotechnical properties: liquid prevents the formation of a graphite film on the counterbody but reduces the coefficient of friction by penetrating between the mating elements [10–12]. Additionally, impregnation with modifying agents improves the wear resistance of antifriction materials [7–9, 13, 14].

To further enhance performance characteristics, nanomaterial additives are introduced into antifriction materials. Carbon nanostructures (CNSs) have proven to be universal fillers for composites used in the aerospace, automotive, and construction industries, as well as in medicine, electronics, and other fields [15, 16]. However, CNSs are highly prone to aggregation, which necessitates finding optimal parameters for their incorporation into composites. For example, in [17], the uniformity of carbon nanotube (CNT) dispersion in a copper-based antifriction material matrix was improved by oxidation with a mixture of sulfuric and nitric acids, leading to a reinforced composite with enhanced strength and tribotechnical properties. In [18], a synergistic effect was observed from the introduction of a boron carbide and CNT mixture, resulting in reduced and stabilized friction coefficients and improved wear resistance of the antifriction material. A similar effect was noted in [19] when CNTs modified with zinc methacrylate were used in a rubber-based composite.

Carbon nanofibers (CNFs), which possess high strength, flexibility, and a developed specific surface area [20], are also used in composite materials. For instance, in [21], it was shown that the introduction of CNFs into a copper matrix reduced the friction coefficient by a factor of eight compared to pure copper. The addition of 6 wt. % CNFs to a poly-α-olefin-based lubricant reduced counterbody wear and extended the service life of wind turbines [9].

Graphene oxide (GO), another representative of CNSs, consists mainly of sp^2-hybridized carbon atoms. However, unlike classical graphene, GO contains a large number of oxygen-containing functional groups (hydroxyl, carboxyl, epoxy, etc.). In [22], it was demonstrated that adding a mixture of reduced graphene oxide (rGO) and aluminum oxide improves the wear resistance of tungsten carbide. The introduction of a mixture of N-cyclohexyl-benzothiazole-2-sulfonamide and GO enhances the physical-mechanical, thermal, and tribotechnical properties of rubber-based composites [23].

The authors of [24] reported a tenfold reduction in the friction coefficient when a mixture of GO and zinc ferrite was added to poly-α-olefin.

Thus, CNSs frequently exhibit positive effects when used as fillers in tribotechnical composite materials based on various matrices. The aim of this study is to evaluate the feasibility of using graphene oxide in a graphite-based antifriction material, as well as to optimize the composition of components through mathematical modeling and to investigate the structure and physical-mechanical properties of the resulting composite.

2. Materials and Methods

2.1. Initial materials

The raw components used for the preparation of the composite material included fine-grained graphite of grade MPG-7 ($\rho = 2.15$ g·cm^{-3}) produced by JSC "NIIGraphite" (TC 1915-051-00200851) and natural graphite GAK-1 ($\rho = 2.25$ g·cm^{-3}) from the Taiginsky deposit (Russian Standard 17022–81). Coal tar pitch, a high-temperature binder, was obtained from LLC "Mini-Max" (Russian Standard 1038–2023). The nanomodifier used was graphene oxide produced by LLC "Nanotechcenter", Tambov, supplied as a 1 wt. % aqueous suspension.

2.2. Preparation of experimental samples

The methodology for obtaining experimental samples included preliminary raw material crushing, co-milling of graphite and GO in a vibratory mill (batch preparation), extrusion mixing with the binder, crushing, preparation of press powder, pressing, and firing. The GO suspension content in the MPG-7 and GAK-1 mixture varied from 0 to 1.6 wt. %.

2.3. Analytical methods

The adsorption capacity of the initial and GO-modified batch in relation to pitch (A, mg·m^{-2}) was determined by measuring the light absorption of a pitch solution in toluene before (D_0) and after (D_1) contact with the filler using a FEK-56 photoelectric colorimeter (JSC "Zagorsk optical and mechanical plant") at a filter wavelength of 540 nm. The pitch concentrations (C_0 and C_1) corresponding to the optical densities (D_0) and (D_1) were determined using a calibration curve. The adsorption capacity A of the filler was calculated using the formula:

$$A = \frac{(C_0 - C_1)V}{m\,S_{\text{BET}}}, \qquad (1)$$

where C_0 – concentration of the initial pitch solution in toluene, mg·mL^{-1}; C_1 – concentration of the pitch solution in toluene after contact with the filler filler, mg·mL^{-1}; V – volume of the pitch solution in toluene, mL; m – mass of the filler sample, g; S_{BET} – specific surface area, m^2·g^{-1}.

The morphology of the batch was examined using scanning electron microscopy (SEM) with a FlexSEM 1000 II (Hitachi) equipped with a tungsten cathode at an accelerating voltage of 20 kV.

Raman spectra of the batch were recorded using a DXR Raman Microscope (Thermo Scientific) with a laser wavelength of 532 nm. X-ray diffraction (XRD) patterns were obtained using an ARL Equinox 1000 (Thermo Scientific) equipped with a Cu-anode X-ray tube (wave length – 1.5406 Å).

The granulometric composition of the batch was determined using a Mastersizer 3000 laser particle size analyzer (Malvern Instruments Ltd.). The specific surface area was measured using nitrogen adsorption at 77 K on an ASAP 2020 (Micromeritics) using the BET method. Vibrational density was determined according to Russian Standard 25279-93 using a Dual Autotap device.

The compressive strength of the samples was determined using a Zwick/Roell Z250 testing machine based on the maximum load and the stress developed in the sample cross-section.

3. Results and Discussion

3.1. Optimization of the batch formulation

To optimize the batch formulation of the newly developed antifriction self-lubricating graphite-based material, a mathematical experimental design method was applied. The investigated variables included the following components: MPG-7 graphite (X_1), natural graphite GAK-1 (X_2), and GO suspension (X_3). Table 1 presents the feasible variation limits for these components.

Table 1. Limits of change in concentration of components

Components, wt. %	MPG-7 graphite (X_1)	Natural graphite GAK-1 (X_2)	GO suspension (X_3)
Minimum content	81.5	9	0
Maximum content	92	15	1.6

To reduce the factorial space and simplify the computational procedure when planning the experiment, the dependence of the key optimization parameter was considered in terms of the ratio of components rather than their absolute quantities. Based on the variable limits in absolute values, the factor constraints Z_j were calculated as follows:

$$Z_j^{\min} \le Z_j \le Z_j^{\max};$$

$$Z_j^{\min} = \frac{X_{i\min}}{X_{1\max}};\ Z_j^{\max} = \frac{X_{i\max}}{X_{1\min}}, \qquad (2)$$

where $j = 1, \ldots, 2$; $X_{i\,\min}$, $X_{i\,\max}$ – the absolute values of the variable X_i at the lower and upper boundaries, respectively.

When using component ratios as factors in the mixture, the following values were determined sequentially:

– center coordinates using the equation:

$$Z_j^0 = \frac{Z_j^{\min} + Z_j^{\max}}{2}; \qquad (3)$$

– variation intervals:

$$\Delta Z_j = \frac{Z_j^{\min} - Z_j^{\max}}{2}. \qquad (4)$$

Next, the coded variables (δ_j) were recorded so that their values varied within the interval –1÷1:

$$\delta_j = \frac{Z_j - Z_j^0}{\Delta Z_j}. \qquad (5)$$

Thus, the experimental design was recorded in three forms: for the coded variables δ_j, for the component ratios Z_j, and for the natural variables X_i. The latter was the most convenient for practical implementation of the experiment. Therefore, for experimental execution, the transition from δ_j to Z_j was carried out using the following formulas:

$$Z_j = Z_j^0 + \delta_j \Delta Z_j; \qquad (6)$$

$$X_1 = \frac{1}{\sum_1^2 Z_j + 1}; \qquad (7)$$

$$X_2 = X_1 Z_1; \qquad (8)$$

$$X_3 = X_1 Z_2. \qquad (9)$$

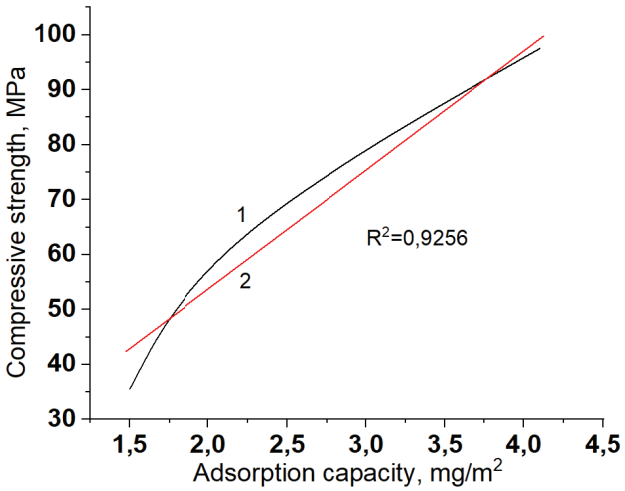

Fig. 1. Dependence of ultimate compressive strength on adsorption capacity:
1 – experimental dependence; *2* – linear dependence

The key optimization parameter chosen was the adsorption capacity of the batch mixture in relation to pitch (*A*). This is one of the critical parameters for assessing the interaction between the filler and the binder, which, in turn, affects the mechanical strength of the final carbon-graphite material (Fig. 1).

At the first stage of experiment planning, the hypothesis regarding the linearity of the regression model was tested. Based on the conducted experiments, a linear regression equation was obtained to describe the dependence of the studied property on the controlled factors $y = 2.28 - 0.03\delta_1 + 0.08\delta_2$ (Fig. 2). As a result of testing the hypothesis for model adequacy, the linear model was rejected.

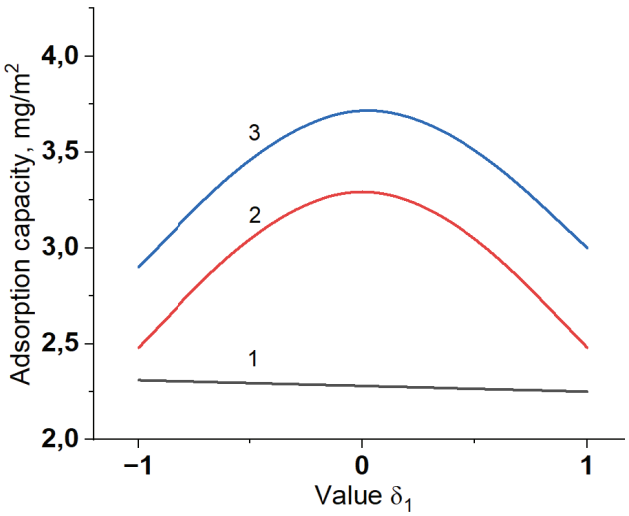

Fig. 2. Values of the adsorption capacity functions at $\delta_2 = 0$:
1 – linear dependence; *2* – quadratic dependence;
3 – measured values

Table 2. Experimental conditions

No.	Coded variables		Relative values of components		Absolute values of components			A, mg·m^{-2}
	δ_1	δ_2	Z_1	Z_2	X_1	X_2	X_3	
1	+	–	0.1890	0	84.1	15.9	0	1.5
2	–	+	0.0997	0.0196	89.3	8.9	1.8	1.7
3	+	0	0.1890	0.0098	83.4	15.8	0.8	3.0
4	–	0	0.0997	0.0098	90.1	9.0	0.9	2.9
5	0	+	0.1443	0.0196	85.9	12.4	1.7	2.0
6	0	–	0.1443	0.0098	87.4	12.6	0	1.5
7	0	0	0.1443	0.0098	86.6	12.5	0.9	4.1

To develop a nonlinear regression equation, the Hartley plan [25] for two factors was chosen as the experimental design, consisting of seven experiments. This plan accounts for the curvature of the response surface while maintaining the minimum possible number of experiments, making it one of the simplest designs for a two-dimensional space.

In this design, the factors are varied at three levels, allowing for the development of a second-order model. Table 2 presents the experimental design matrix for the coded variables δ_i, factors Z_i, and natural values X_i, along with the adsorption capacity values obtained from implementing the described plan.

The response surface was described using a second-order regression equation [25]:

$$y = b_0 + \sum_{i=1}^{2} b_i \delta_i + \sum_{i,j=1}^{2} b_{ij} \delta_i \delta_j + \sum_{i=1}^{2} b_{ii} \delta_i^2. \qquad (10)$$

Based on the experimental data obtained using the Hartley plan, the coefficients of the regression equation were calculated using the following formulas (11) – (14):

$$b_0 = \frac{a}{N} \sum_{u=1}^{N} y_u - \frac{b}{N} \sum_{i=1}^{k} \sum_{u=1}^{N} \delta_{iu}^2 y_u; \qquad (11)$$

$$b_i = \frac{1}{N\lambda_2} \sum_{u=1}^{N} \delta_{iu}^2 y_u; \qquad (12)$$

$$b_{ij} = \frac{1}{N\lambda_3} \sum_{u=1}^{N} \left(\delta_i \delta_j\right)_u y_u; \qquad (13)$$

$$b_{ii} = \frac{c}{N} \sum_{u=1}^{N} \delta_{iu}^2 y_u - \frac{d}{N} \sum_{i=1}^{k} \sum_{u=1}^{N} \delta_{iu}^2 y_u - \frac{b}{N} \sum_{u=1}^{N} y_u. \qquad (14)$$

Additional constants were calculated using the following equations (15) – (18):

$$a = \frac{k\lambda_2^2}{\lambda_4 - \lambda_3 + k\lambda_3 - k\lambda_2^2} + 1; \qquad (15)$$

$$b = \frac{\lambda_2}{\lambda_4 - \lambda_3 + k\lambda_3 - k\lambda_2^2}; \qquad (16)$$

$$c = \frac{1}{\lambda_4 - \lambda_3}; \qquad (17)$$

$$d = \frac{\lambda_3 - \lambda_2^2}{(\lambda_4 - \lambda_3)\left(\lambda_4 - \lambda_3 + k\lambda_3 - k\lambda_2^2\right)}. \qquad (18)$$

Even moments were determined using the following formulas (19) – (21):

$$\lambda_2 = \frac{\sum_{u=1}^{N} \delta_{iu}^2}{N}; \qquad (19)$$

$$\lambda_3 = \frac{\sum_{u=1}^{N} \left(\delta_i^2 \delta_j^2\right)_u}{N}; \qquad (20)$$

$$\lambda_4 = \frac{\sum_{u=1}^{N} \delta_{iu}^4}{N}. \qquad (21)$$

To determine the significance of regression coefficients, their absolute values were compared with the confidence interval, calculated as:

$$\Delta b_i = t_{\alpha,f} S_{b_i}. \qquad (22)$$

The calculated values of the coefficients and their confidence intervals are presented in Table 3.

Table 3. Values of regression coefficients and confidence intervals

Coefficient Value	b_0	b_1	b_2	b_{12}	b_{11}	b_{22}
b_i	3.7	–0.03	0.18	–1.6	–1.22	–2.66
Δb_i	0.21	0.09	0.09	0.17	0.21	0.21

A coefficient is considered statistically insignificant if its absolute value is smaller than its confidence interval.

Comparing the confidence intervals with the absolute values of the regression coefficients showed that only coefficient b_1 was statistically insignificant. Therefore, it was excluded from the model.

As a result, the following mathematical model (23) was obtained, which meets the adequacy requirement:

$$y = 3.7 + 0.18\delta_2 - 1.6\delta_1\delta_2 - 1.22\delta_1^2 - 2.66\delta_2^2. \quad (23)$$

For further analysis, the mathematical model was transformed into its canonical form (24):

$$y - 3.7 = -3.01\tilde{\delta}_1^2 - 0.87\tilde{\delta}_2^2. \quad (24)$$

Since the coefficients have the same sign, the response surface is an ellipsoid, and its center is an extremum (maximum).

The center coordinates are (0; 0), which corresponds to the composition described in the 7th row of the Hartley plan, meaning it represents the optimal formulation of the filler (Fig. 3). Thus, to study the effect of introducing graphene oxide (GO) into the filler composition on the structure, morphology, and physico-mechanical properties of carbon-graphite composites, experimental samples were prepared according to the formulations in the 5th, 6th, and 7th rows of the Hartley plan**.**

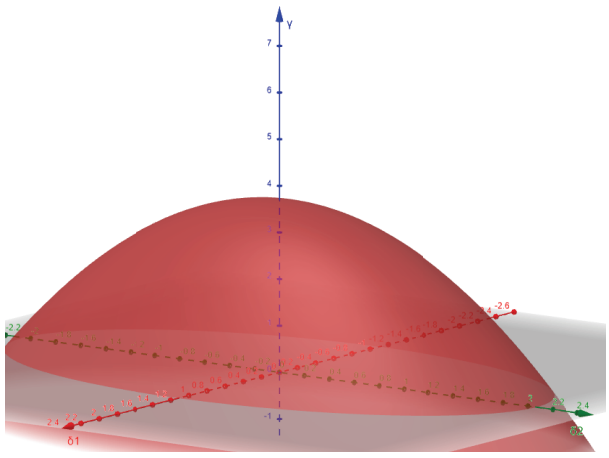

Fig. 3. Response surface in canonical form

3.2. Structure and morphology of nanomodified fillers

Figure 4 presents SEM images of both unmodified and graphene oxide-modified filler samples.

In the volume of the original sample, predominantly round-shaped structural units are identified, corresponding to the morphology of MPG-7, with some inclusions of plate-like shapes typical for GAK-1 particles (Fig. 4*a* and 4*b*).

The sample obtained by adding 0.9 wt. % graphene oxide suspension to the mixture of MPG-7 and GAK-1 exhibits a different structure (Fig. 4*c* and 4*d*). It consists of agglomerated particles of irregular shape. Separate platelets of natural graphite are almost absent here.

As the GO content in the modified filler increases, round and plate-like particles start to appear again on the SEM image (Fig. 4*e* and 4*f*). In this case, the sample is characterized by slightly greater dispersion compared to the unmodified mixture.

Thus, at low concentrations, graphene oxide promotes the binding of graphite components, whereas at higher concentrations, it causes de-agglomeration and separation of individual particles.

This assumption is confirmed by the data on the particle size distribution of the batch, obtained using a laser particle size analyzer (Fig. 5). Indeed, the sample made from the mixture containing 0.9 wt. % GO has fewer small particles and more larger particles compared to the unmodified filler. The material obtained from the mixture with 1.7 wt. % GO exhibits the highest dispersion.

Additional information about the changes in the filler structure during nanomodification was obtained based on the specific surface area and vibrational density (ρ_v) values (Table 4). The ρv values indicate that, when 0.9 wt. % GO is introduced, a denser grain of filler is formed with fewer voids, which in turn promotes a tighter packing of the particles.

Moreover, the introduction of 0.9 wt. % by weight of GO likely contributes to the closure of pores in the material, which leads to a reduction in specific surface area by a factor of 3.5. The increase in the specific surface area of the filler with a higher GO content is related to the deagglomeration of particles.

One contradiction is that the more dispersed nanomodified sample with 1.7 wt. % GO has a lower specific surface area than the unmodified filler. It can be assumed that this is due to the increase in the true density of the material during nanomodification.

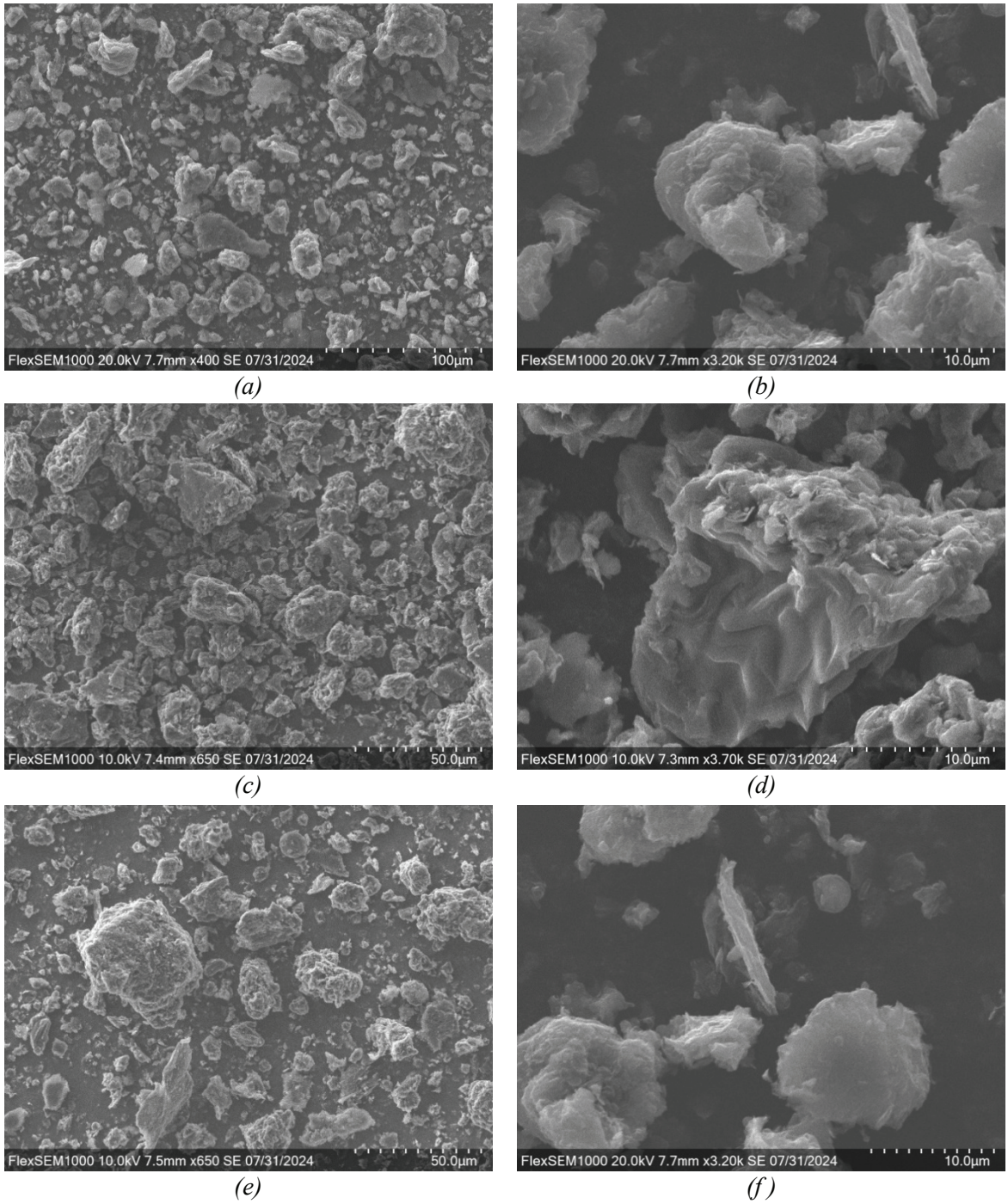

Fig. 4. SEM images of filler samples obtained from mixtures with GO suspension content equal to 0 (*a*, *b*), 0.9 (*c*, *d*) and 1.7 (*e*, *f*) wt. %

Traditionally, the method of X-ray phase analysis is used to evaluate the changes in the volumetric structure of graphite materials [27]. The X-ray diffractogram of natural graphite GAK-1 (Fig. 6) has a typical appearance. The most intense peak corresponds to the crystallographic plane (002) at $2\theta = 26°$ with an interplanar distance (d_{002}) of 3.42 Å. The second signal on the diffractogram near 54° is much less intense and can be decomposed into two components with closely spaced peaks at 53.5° ($d_{004} = 1.71$ Å) and 54.1° ($d_{004} = 1.69$ Å). Both of these values correspond to the crystallographic plane (004). This suggests that the material contains a less structured phase, characterized by a higher d_{004} value.

The X-ray diffractogram of the MPG-7 material contains a set of peaks characteristic of highly ordered fine crystalline graphite at 2θ values of 26.3° (002), 42° (100), 44° (101), 54° (004), 78° (110), and 84° (112).

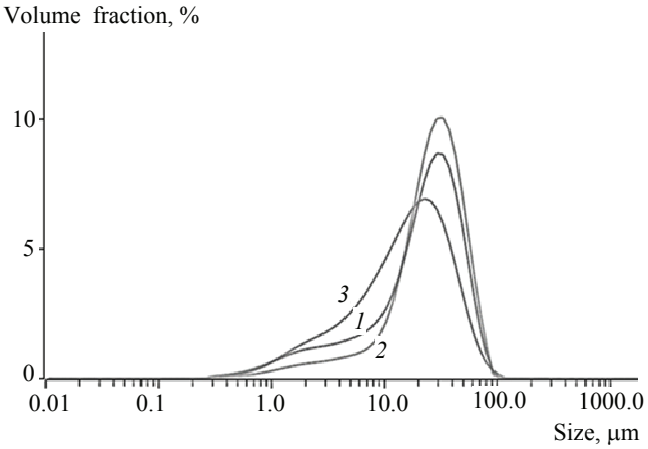

Fig. 5. Particle size distribution in charge samples: unmodified (*1*) and obtained from a mixture containing 0.9 (*2*) and 1.7 (*3*) wt. % exhaust gas suspension

Table 4. Properties of fillers

GO content, wt. %	ρ_v, g·cm^{-3}	Specific surface area, m^2·g^{-1}
0	0.73	29.10
0.9	0.78	8.06
1.6	0.74	17.45

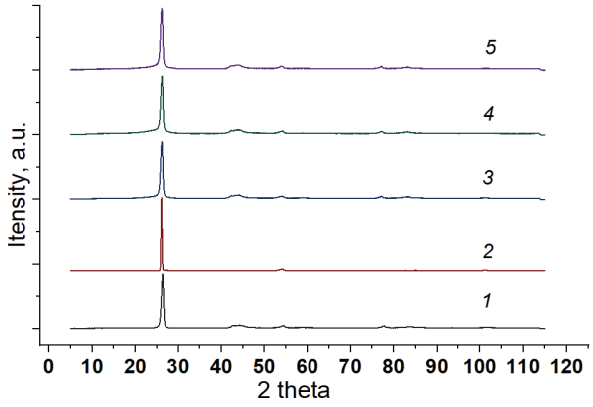

Fig. 6. X-ray diffractograms of samples of synthetic graphite (*1*), natural graphite (*2*) and charge obtained from a mixture containing 0.9 (*3*) and 1.7 wt. % (*4*) of graphene oxide suspension

All three samples of the charge demonstrate a diffraction pattern characteristic of the predominant component of the mixture – artificial graphite MPG-7. There are only slight differences between the samples in the values of interplanar distances (Table 5), calculated using the Wulf-Breig equation. In the unmodified and modified charge samples, the values of d are slightly higher than in MPG-7. The filler made from the mixture containing 0.9 wt. % GO suspension has the lowest values of d_{100} and d_{004} among the three samples.

Table 5. Results of X-ray phase analysis of initial graphites and charge samples

Sample	Interplanar distance, Å					
	d_{002}	d_{100}	d_{101}	d_{004}	d_{110}	d_{112}
GAK-1	3.35	–	–	1.69–1.71	–	–
MPG-7	3.38	2.11	2.05	1.68	1.22	1.16
Unmodified charge	3.40	2.14	2.06	1.70	1.24	1.16
Charge from a mixture containing 0.9 wt. % GO suspension	3.40	2.13	2.06	1.69	1.24	1.16
Charge from a mixture containing 1.7 wt. % GO suspension	3.40	2.14	2.06	1.70	1.24	1.16

However, overall, the differences are so small that it can be said that the volumetric structure of all the charge samples is similar.

Figure 7 shows the Raman spectra (RS) of the investigated filler samples. The spectra exhibit peaks characteristic of carbon materials, and the position and intensity of these peaks can be used to assess the parameters and nature of surface defects.

The D peak (~1350 cm^{-1}) is the breathing mode A_{1g} [28], associated with defects in the basic structure. The G peak (~1550 cm^{-1}) is due to in-plane vibrations of carbon atoms in graphene sheets with E_{2g} symmetry [29]. In the Raman spectrum of GAK-1, the D peak is almost absent, indicating the well-ordered structure of its surface graphene layers. In the spectrum of MPG-7, the intensity of this peak is higher, likely due to the fragmentation of the material and the high proportion of edge areas on the surface of the particles that make it up.

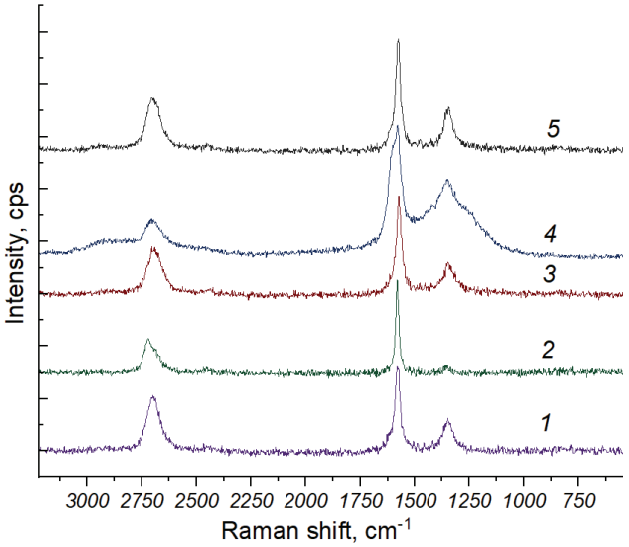

Fig. 7. Raman spectra of synthetic graphite MPG-7 (*1*), natural graphite GAK-1 (*2*) and charge samples obtained from mixtures with GO suspension content equal to 0 (*3*), 0.9 (*4*) and 1.7 (*5*) wt. %.

Additionally, on the spectra of all analyzed samples, there is a relatively intense 2D band (~2700 cm^{-1}), which is characteristic of zone-boundary phonons of the second order and indicates the formation of a graphene-like structure [30]. Overall, the general appearance of the Raman spectra and the ratios of the characteristic peak heights are quite typical for graphite materials [31].

In the Raman spectra of the nanomodified charge, a broad D + G peak also appears with a blurred peak around 2900 cm^{-1} [32], more intense for the sample with 0.9 wt. % graphene oxide. The appearance of this band indicates the disorder and defects in the surface graphene layers of the material.

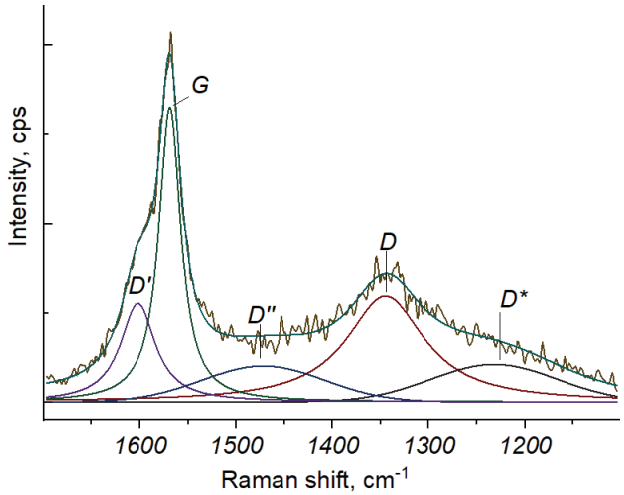

Fig. 8. Fragment of Raman spectra of charge sample containing 0.9 wt. % of GO suspension with deconvolution of main peaks

The D peak is also most intense in the spectrum of the sample from the charge obtained from the original mixture containing 0.9 wt. % graphene oxide. Therefore, this confirms the assumption of a higher number of defects in the graphene layers of this sample compared to the other materials. This fact, along with the change in the height and symmetry of the 2D peak, may indicate the amorphization of the surface structure [33].

By decomposing the D and G peaks using Lorentzian functions ($OMNIC_{TM}$) software), the peaks D', D", and D* were identified within them (Fig. 8). The validity of this approach for interpreting Raman spectroscopy data is discussed in [34]. The highest intensity of the D' peak (~1620 cm^{-1}) in the spectrum of the sample containing 0.9 wt. % graphene oxide indicates a significant number of carbon atoms in an sp^3hybridization state on the surface of the granules [35]. The D" peak (~1500 cm^{-1}) is associated with the presence of lattice defects in graphite [36]. The broadening of the G-band in this spectrum may be due to the presence of hydroxyl and epoxy groups [37], which are components of graphene oxide. This is also indicated by the presence of the D* peak [38, 39].

Table 6 presents the results of Raman spectroscopy data analysis. These results confirm the previously mentioned assumptions about the changes in the structure of the filler when different amounts of graphene oxide are introduced into its composition. The sample containing 0.9 wt. % graphene oxide is characterized by the maximum values of the D/G and D"/G ratios, which are used to assess the degree of defectiveness and overall disorder of the surface of graphite materials. It should be noted that the values of D"/G and D*/G decrease as the graphene oxide content in the nanomodified charge increases. This may be because graphene oxide contributes to more effective dispersion of the graphite components during mechanical processing in the vibratory mill. The microflakes of graphite components formed as a result of this process may screen (cover) the oxygen-containing groups of graphene oxide. Another noteworthy observation is that for the unmodified charge, the D/D' ratio is 13, which is characteristic of a predominance of sp^3 defects on the surface, whereas for the nanomodified charges of both compositions, the D/D' ratio is close to 3.5, indicating that edge defects are predominant [40]. This can also be explained by the fact that the graphite flakes cover the surface of the larger particles.

Thus, the sample of the nanomodified filler obtained from the mixture containing 0.9 wt. % graphene oxide, with the highest density and lowest

Table 6. Results of Raman spectroscopy data processing

Sample	Ratio of peak intensities (areas) in Raman spectra				
	D/G	2D/G	D/D’	D*/G	D’/G
GAK-1	0.428	1.224	–	–	–
MPG-7	0.061	1.129	–	–	–
Unmodified charge	0.739	1.377	13	–	0.062
Charge from a mixture containing 0.9 wt. % GO suspension	1.811	1.406	3.5	0.452	0.452
Charge from a mixture containing 1.7 wt. % GO suspension	0.792	1.458	3.5	0.057	0.065

pecific surface area, contains the greatest number of defects, which can facilitate its interaction with the binder (pitch).

3.3. Physical and mechanical characteristics of experimental samples

Photographs of the final carbon-graphite composites, obtained using both the original and nanomodified charge, are shown in Fig. 9. There are virtually no external differences between them.

Table 7 presents the physical and mechanical characteristics of the experimental samples: density before and after firing (ρ_{pr} and ρ_f, respectively), the changes in mass and volume of the materials observed during firing, and the compressive strength limit (σ) of the final nanocomposite.

Analysis of these data shows that the unmodified sample is characterized by the densest grain packing after molding. This is likely due to the absence of graphene oxide layers between the particles. The low density of the pressed sample containing 0.9 wt. % graphene oxide in the filler may be related to both the greater anisometry of the grains and their relatively high stiffness.

It is likely that graphene oxide plays a role in forming bonds between the nanomodified filler and the binder, which results in increased strength properties of the composite. The high adsorption activity per unit surface area of the sample made from the mixture containing 0.9 wt. % graphene oxide is accompanied by relatively larger volumetric changes compared to the other samples.

The reduction in shrinkage in the sample with the filler containing 1.7 wt. % graphene oxide may be due to the excess amount of nanomaterial reacting with the binder to form a rigid framework. At lower graphene oxide content, the nanomodifier (graphene oxide) reduces the contact losses at the filler-binder interface and also contributes to the formation of bonds between the graphite components of the filler.

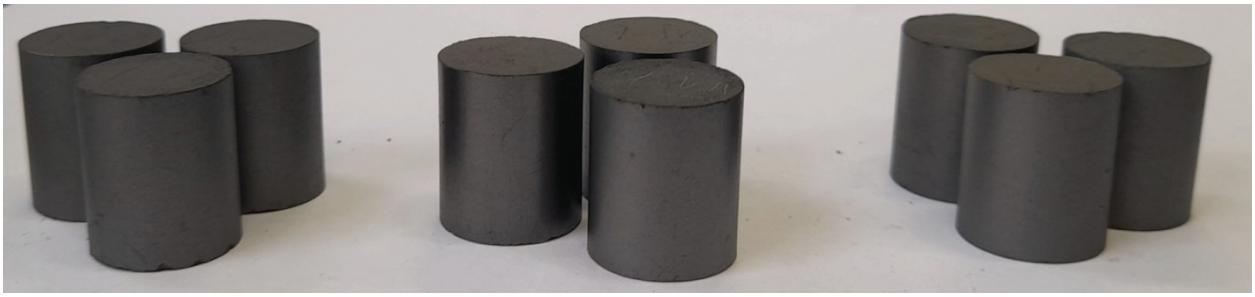

Fig. 9. Samples of finished carbon-graphite composites obtained from unmodified charge (left) and from charges containing 0.9 (center) and 1.7 (right) wt. % graphene oxide

Table 7. Physico-mechanical characteristics of prototypes of carbon-graphite nanocomposite

GO content, wt. %	ρ_{pr}, g·cm^{-3}	ρ_f, g·cm^{-3}	Mass changes, %	Volume changes, %	σ, MPa
0	1.59	1.57	7.11	5.43	35.5
0.9	1.46	1.59	9.70	15.56	97.5
1.6	1.52	1.57	8.56	10.44	63.0

This hypothesis is based on the assumption that, when mixed with 0.9 wt. % graphene oxide, the graphite particles may experience not only weak van der Waals forces but also covalent interactions that contribute to the formation of strong agglomerates. It can be assumed that, in these agglomerates, artificial graphite acts as a "core" chemically bonded to natural graphite via the functional groups of graphene oxide, which are pre-adsorbed on the surface of natural graphite. This interaction is one of the most likely causes of the increased strength of the material after firing.

4. Conclusion

Graphene oxide-modified carbon-graphite composites were produced in this study. A mathematical model was developed to select the optimal component composition and to investigate the structure and physical-mechanical properties of the resulting compositions. Using the Hartley design, the experimental planning was carried out, and the recipes for the graphene oxide-modified filler for the carbon-graphite composite were selected. The effect of nanomodification on changes in the structure and morphology of the filler was analyzed. It was shown that the sample made from the mixture of MPG-7/ GAK-1/GO containing 0.9 wt. % graphene oxide differs from the unmodified filler and the material with higher graphene oxide concentration in terms of defect parameters. The promising use of graphene oxide as a component in antifriction carbon-graphite composites was demonstrated. Further increases in density and compressive strength will be supported by optimizing the component composition and determining the rational processing parameters for grinding and combining them during the formation of the composite.

5. Funding

This research did not receive external funding.

6. Acknowledgements

This work has been done using facilities of the Shared Research Facility "Production and application of multifunctional nanomaterials" (Tambov State Technical University).

7. Conflict of interests

The authors declare no conflicts of interests.

References

1. Kablov EN. Innovative developments of FSUE "VIAM" SSC of RF on realization of «Strategic directions of the development of materials and technologies of their processing for the period until 2030. *Aviatsionnye materialy i tekhnologii*. 2015;(1(34)):3-33. DOI:10.18577/ 2071-9140-2015-0-1-3-33 (In Russ.)

2. Farafonov DP, Migunov VP, Aleshina RSh. Tribotechnical characteristics research of materials used for gas turbine engines blade shroud hardening. *Aviatsionnye materialy i tekhnologii*. 2016;(S1):24-30. DOI:10.18577/2071-9140-2016-0-S1-24-30 (In Russ.)

3. Belogorsky VD. *Antifriction graphite and its application in industry*. Moscow: Znaniye; 1974. 154 p. (In Russ.)

4. Zhao J, Liu L, Guo Q, Shi J, et al. Oxidation protective behavior of SiC/Si–$MoSi_2$ coating for different graphite matrix. *Materials Letters*. 2006;60(16):1964-1967. DOI:10.1016/j.matlet.2005.12.072

5. Sun C, Li H, Luo H, Xie J, et al. Effect of Y_2O_3 on the oxidation resistant of $ZrSiO_4$/SiC coating prepared by supersonic plasma spraying technique for carbon/carbon composites. *Surface and Coatings Technology*. 2013;235:127-133. DOI:10.1016/j.surfcoat. 2013.07.023

6. Konno H, Kinomura T, Habazaki H, Aramata M. Formation of oxidation resistant graphite flakes by ultrathin silicone coating. *Surface and Coatings Technology*. 2005;194(1):24-30. DOI:10.1016/j.surfcoat. 2004.04.079

7. Wang P, Xie F, Wexler D, Yin J, et al. Tribological behaviors of copper modified carbon/carbon composites for pantograph strip under electric current conditions. *Tribology International*. 2023;185:108483. DOI:10.1016/j.triboint.2023.108483

8. Zhang X, Guo R, Guo Y, Ai Y, et al. Sustainable antimony management via porphyrin ligand-based MOFs: from enrichment of antimony from water to the utilization in SBO_2-based aqueous batteries. *Journal of Environmental Chemical Engineering*. 2023;11(6):111148. DOI:10.1016/j.jece.2023.111148

9. Xia R, Lou D, Younes H, Haiston J, et al. Synergistic effect of hexagonal boron nitride and carbon nanofibers on tribological behavior of nanolubricant. *Tribology International*. 2023;177:107957. DOI:10.1016/ j.triboint.2022.107957

10. Xu J, Du J, Gao X, Jiang T, et al. Tribological behaviors and wettability evolution of phenolic resin-impregnated graphite materials under water immersion condition. *Annals of Nuclear Energy*. 2024;208:110792. DOI:10.1016/j.anucene.2024.110792

11. Borruto A, Crivellone G, Marani F. Influence of surface wettability on friction and wear tests. *Wear*. 1998;222(1):57-65. DOI:10.1016/S0043-1648(98)00256-7

12. Golchin A, Friedrich K, Noll A, Prakash B. Influence of counter surface topography on the tribological behavior of carbon-filled PPS composites in water. *Tribology International*. 2015;88:209-217. DOI:10.1016/ j.triboint.2015.03.023

13. Lu J, Ma Y, Shi J, Li H, et al. *Molecular dynamics simulation and test characterization of metal migration behavior in antimony-impregnated graphite*. SSRN. Available from: https://papers.ssrn.com/sol3/papers.cfm?abstract_id=4746340 [Accessed 17 December 2025]

14. Zhang Z, Qiao Z, Wang X, Guo Y, et al. Comparative study on fretting friction and wear characteristics of different impregnated graphite for sealing application. *Wear*. 2024;552-553:205455. DOI:10.1016/j.wear.2024.205455

15. Abbasi S, Peerzada MH, Nizamuddin S, Mubarak NM. Functionalized nanomaterials for the aerospace, vehicle, and sports industries. In: *Handbook of functionalized nanomaterials for industrial applications*. Elsevier; 2020. p. 795-825. DOI:10.1016/B978-0-12-816787-8.00025-9

16. Macías-Silva MA, Cedeño-Muñoz JS, Morales-Paredes CA, Tinizaray-Castillo R, et al. Nanomaterials in construction industry: an overview of their properties and contributions in building house. *Case Studies in Chemical and Environmental Engineering*. 2024;10:100863. DOI:10.1016/j.cscee.2024.100863

17. Trinh PV, Trung TB, Thang NB, Thang BH, et al. Calculation of the friction coefficient of Cu matrix composite reinforced by carbon nanotubes. *Computational Materials Science*. 2010;49(4):S239-S241. DOI:10.1016/j.commatsci.2010.01.035

18. Lai C, Zhong M, Xu W, Yi M, et al. Influences of B_4C and carbon nanotubes on friction and wear performance of Cu base self-lubricating composite. *Tribology International*. 2023;187:108726. DOI:10.1016/j.triboint.2023.108726

19. Han D, Wang L, Zhang S, Zhang Q, et al. The impact of synergistic action of methacrylic acid/zinc oxide/carbon nanotubes on metal friction and wear. *Wear*. 2024;546-547:205342. DOI:10.1016/j.wear.2024.205342

20. Feng L, Xie N, Zhong J. Carbon nanofibers and their composites: a review of synthesizing, properties and applications. *Materials*. 2014;7(5):3919-3945. DOI:10.3390/ma7053919

21. Larionova T, Koltsova T, Fadin Yu, Tolochko O. Friction and wear of copper–carbon nanofibers compact composites prepared by chemical vapor deposition. *Wear*. 2014;319(1-2):118-122. DOI:10.1016/j.wear.2014.07.020

22. Tian X, Liang Y, He G, Zeng L. Reduced graphene oxide and alumina synergistically enhance the mechanical and wear properties of WC-8CO cemented carbide. *International Journal of Refractory Metals and Hard Materials*. 2023;113:106184. DOI:10.1016/j.ijrmhm.2023.106184

23. Yang J, Wang F, Liang C, Zhou S, et al. Surface one-step modification of graphene oxide with n-cyclohexylbenzothiazole-2-sulfonamide to enhance the wear resistance of natural rubber/butadiene rubber composites. *Colloids and Surfaces A: Physicochemical and Engineering Aspects*. 2024;703:135314. DOI:10.1016/j.colsurfa.2024.135314

24. Suresh R, Muthukrishnaraj A, Kumar SP. Green magnetic nanoparticles for tribological application. In: *Green Magnetic Nanoparticles (GMNPs)*. Elsevier; 2024. p. 301-320. DOI:10.1016/B978-0-443-21895-8.00012-6

25. Novik F, Arsov A. *Optimization of metal technology processes by experimental design methods*. Moscow: Mashinostroyeniye; 1980. 304 p. (In Russ.)

26. Badenhorst H. Microstructure of natural graphite flakes revealed by oxidation: limitations of XRD and Raman techniques for crystallinity estimates. *Carbon*. 2014;66:674-690. DOI:10.1016/j.carbon.2013.09.065

27. Zhang HB, Zheng WG, Yan Q, Yang Y, et al. Electrically conductive polyethylene terephthalate/graphene nanocomposites prepared by melt compounding. *Polymer*. 2010;51(5):1191-1196. DOI:10.1016/j.polymer.2010.01.027

28. Jaafar E, Kashif M, Sahari SK, Ngaini Z. Study on morphological, optical and electrical properties of graphene oxide (GO) and reduced graphene oxide (RGO). *Materials Science Forum*. 2018;917:112-116. DOI:10.4028/www.scientific.net/MSF.917.112

29. Kamel MSA, Stoppiello CT, Jacob MV. Improved transfer-free sustainable graphene electrode using silver nanowires for organic photovoltaics. *ACS Applied Energy Materials*. 2023;6(21):11168-11178. DOI:10.1021/acsaem.3c02001

30. Abyzov AM, Ivanova EA, Smirnov EP. Raman spectroscopic study of sp^2-carbon materials. *Neorganicheskiye materialy = Inorganic Materials*. 1987;23(10):1664-1668. (In Russ.)

31. Kamel MSA, Oelgemöller M, Jacob MV. Chemical vapor deposition-grown graphene transparent conducting electrode for organic photovoltaics: advances towards scalable transfer-free synthesis. *Renewable and Sustainable Energy Reviews*. 2024;203:114740. DOI:10.1016/j.rser.2024.114740

32. Ferrari AC, Robertson J. Resonant Raman spectroscopy of disordered, amorphous, and diamondlike carbon. *Physical Review B*. 2001;64(7):075414. DOI:10.1103/PhysRevB.64.075414

33. Chernyak SA, Ivanov AS, Stolbov DN, Egorova TB, et al. N-doping and oxidation of carbon nanotubes and jellyfish-like graphene nanoflakes through the prism of Raman spectroscopy. *Applied Surface Science*. 2019;488:51-60. DOI:10.1016/j.apsusc.2019.05.243

34. Scardaci V, Compagnini G. Raman spectroscopy data related to the laser induced reduction of graphene oxide. *Data in Brief*. 2021;38:107306. DOI:10.1016/j.dib.2021.107306

35. Radoń A, Włodarczyk P, Łukowiec D. Structure, temperature and frequency dependent electrical conductivity of oxidized and reduced electrochemically exfoliated graphite. *Physica E: Low-dimensional Systems and Nanostructures*. 2018;99:82-90. DOI:10.1016/j.physe.2018.01.025

36. Pimenta MA, Dresselhaus G, Dresselhaus MS, Cançado LG, et al. Studying disorder in graphite-based systems by Raman spectroscopy. *Physical Chemistry*

Chemical Physics. 2007;9(11):1276-1290. DOI:10.1039/B613962K

37. Eckmann A, Felten A, Mishchenko A, Britnell L, et al. Probing the nature of defects in graphene by Raman spectroscopy. *Nano Letters*. 2012;12(8):3925-3930. DOI:10.1021/nl300901a

38. Wu JB, Lin ML, Cong X, Liu HN, et al. Raman spectroscopy of graphene-based materials and its applications in related devices. *Chemical Society Reviews*. 2018;47(5):1822-1873. DOI:10.1039/C6CS00915H

39. Anusuya T, Pathak DK, Kumar R, Kumar V. Deconvolution and quantification of defect types from the first order Raman spectra of graphene oxide derivatives. *FlatChem*. 2022;35:100422. DOI:10.1016/j.flatc.2022.100422

40. Cheng Y, Yang L, Fang C, Guo X. Co-carbonization behavior of petroleum pitch/graphene oxide: influence on structure and mechanical property of resultant cokes. *Journal of Analytical and Applied Pyrolysis*. 2016;122:387-394. DOI:10.1016/j.jaap.2016.08.019

Information about the authors / Информация об авторах

Roman D. Balabanov, Postgraduate Student, Tambov State Technical University (TSTU), Tambov, Russian Federation; Junior Researcher, JSC NIIgrafit, Moscow, Russian Federation; ORCID 0009-0001-2946-3119; e-mail: balabanoff@gmail.com

Tatyana P. Dyachkova, D. Sc. (Chem.), Professor, TSTU, Tambov, Russian Federation; ORCID 0000-0002-4884-5171; e-mail: dyachkova_tp@mail.ru

Anna G. Fedyushkina, Head of Department, JSC NIIgrafit, Moscow, Russian Federation; ORCID 0009-0009-8987-9851; e-mail: AGFedyushkina@rosatom.ru

Irina V. Gutnik, Cand. Sc. (Eng.), Associate Professor, TSTU, Tambov, Russian Federation; ORCID 0000-0003-1236-7187; e-mail: i.v.gutnik@yandex.ru

Georgy A. Titov, Student, TSTU, Tambov, Russian Federation; ORCID 0000-0002-3930-0559; e-mail: bombercd1@mail.ru

Elena A. Burakova, D. Sc. (Eng.), Associate Professor, TSTU, Tambov, Russian Federation; ORCID 0000-0001-8927-7433; e-mail: elenburakova@yandex.ru

Evgeny N. Tugolukov, D. Sc. (Eng.) Professor, TSTU, Tambov, Russian Federation; ORCID 0000-0003-1766-3786; e-mail: tugolukov.en@mail.ru

Балабанов Роман Дмитриевич, аспирант, Тамбовский государственный технический университет (ТГТУ), Тамбов, Российская Федерация; младший научный сотрудник, АО «НИИграфит», Москва, Российская Федерация; ORCID 0009-0001-2946-3119; e-mail: balabanoff@gmail.com

Дьячкова Татьяна Петровна, доктор химических наук, профессор, ТГТУ, Тамбов, Российская Федерация; ORCID 0000-0002-4884-5171; e-mail: dyachkova_tp@mail.ru

Федюшкина Анна Генриховна, руководитель направления, АО «НИИграфит», Москва, Российская Федерация; ORCID 0009-0009-8987-9851; e-mail: AGFedyushkina@rosatom.ru

Гутник Ирина Владимировна, кандидат технических наук, доцент, ТГТУ, Тамбов, Российская Федерация; ORCID 0000-0003-1236-7187; e-mail: i.v.gutnik@yandex.ru

Титов Георгий Анатольевич, студент, ТГТУ, Тамбов, Российская Федерация; ORCID 0000-0002-3930-0559; e-mail: bombercd1@mail.ru

Буракова Елена Анатольевна, доктор технических наук, доцент, ТГТУ, Тамбов, Российская Федерация; ORCID 0000-0001-8927-7433; e-mail: elenaburakova@yandex.ru

Туголуков Евгений Николаевич, доктор технических наук, профессор, ТГТУ, Тамбов, Российская Федерация; ORCID 0000-0003-1766-3786; e-mail: tugolukov.en@mail.ru

Received 15 January 2025; Revised 13 February 2025; Accepted 17 February 2025